AN IMPLICIT SOLUTION OF THE UNSTEADY NAVIER-STOKES EQUATIONS ON UNSTRUCTURED MOVING GRIDS

Alireza Jahangirian *, Mostafa Hadidoolabi *
*** Aerospace Engineering Department**
Amirkabir University of Technology
Tehran, Iran

Keywords: *Implicit method, Unsteady viscous flows, Unstructured moving grids*

Abstract

An efficient dual-time implicit approach combined with the unstructured moving grids is presented for solution of the unsteady turbulent flows. Unstructured grids suitable for both inviscid and turbulent viscous flow regions are generated using a successive refinement method and the grid is moved adaptively based on the boundary movements. Special care is taken to maintain the quality of the grid near the surface. The unsteady two-dimensional compressible Navier-Stokes equations are discretised by an implicit approach in a real time basis. This approach allows the real time step to be chosen on the basis of accuracy rather than stability thus, enabling the use of large CFL numbers for computational efficiency. The resulting set of implicit non-linear equations is then solved iteratively in a pseudo-time using a Runge-Kutta scheme. The $k-\varepsilon$ turbulence model equations are solved together with the main flow equations in a fully coupled manner. Results are presented for two unsteady test cases oscillating airfoils and comparisons with the experimental data showed good agreements.

1 Introduction

A great variety of flows with significance to aerodynamic applications are inherently unsteady, including bluff body wakes, turbine and rotor flows, store separation and aeroelastic problems. Most of these applications are concerned with the complex geometries including considerable moving boundaries at high Reynolds number flow conditions. Efforts in CFD community have, therefore been towards the efficient procedures for moving grid generation and unsteady flow solution algorithms in order to achieve the required accuracy with reduced computational effort.

A number of calculations have been carried out using the explicit methods [1]. However, the numerical stability restriction imposed to the maximum allowable time step would increase the computational effort particularly in viscous calculations where the ratio of the maximum to the minimum size of the cells can span several orders of magnitude. Implicit methods in contrast allow the use of much larger time steps leading to the significant efficiency for viscous flows. Several implicit methods have been developed, however the implicit dual-time method described by Jameson [2] allows an implicit discretisation to be used in real time, while at each real time step marches the solution in a pseudo-time through an explicit time marching scheme. This method was successfully implemented for solution of inviscid flow around rigid [2] and moving boundaries [3] on structured grids. However, the geometry complexity involved in the aerodynamic applications requires more flexible, unstructured grids to be used. In addition, despite inviscid models yield a cost effective approximation to the solution of unsteady problems, when strong shocks and

separated flows are involved, it is necessary to incorporate viscosity and turbulent effects into the model. Alonso et al. [4] used a zero-equation Baldwin-Lomax turbulence model while, Badcock et al. [5] have chosen a $k-\varepsilon$ two equation turbulence closure. Chassaing et al. [6] utilized the more soffisticated Reynolds stress model. Despite promising results, all of these works have been carried out on the structured grids.

Using unstructured grids for accurate and efficient calculation of high Reynolds number turbulent flows was just recently reported [7], [8] and mostly for steady state flow calculations. Thus, the objective of the present work is development of an implicit unstructured moving grid approach for application to unsteady turbulent Navier-Stokes calculations.

2 Unstructured Moving Grid Generation

Unstructured grids suitable for both inviscid and viscous flow regions are generated based on a combination of grid enrichment procedures, whereby new grid points and point connectivities are created simultaneously [7]. A novel feature of the method is that it does not require an initial distribution of grid points within the flow domain. Also, unlike the majority of the existing methods, which start with a well-refined distribution of the geometry, the present approach adopts a very crude initial discritisation of the geometry and the outer boundary of the domain. Surface and field grids are then generated simultaneously as the cell sub-division process continues. More details about this method can be found in reference [7] and would not be mentioned here. In figure 1 generated grid around NACA64010 airfoil by this method is shown. The grid is then moved adaptively based on the boundary movements using a modified spring analogy approach that maintain the quality of the grid near the surface. This approach also allows geometric deflections required by large CFL numbers of the implicit solution methods. Figure 2, shows the unstructured viscous grid generated around NACA 0012 airfoil before and after movement. As illustrated the quality of the grid inside the viscous layer is preserved during mesh movement process.

3 Numerical Flow Solutions

The two-dimensional Reynolds-averaged unsteady compressible Navier-Stokes equations, can be written in a cartesian coordinate system as:

$$\frac{\partial Q}{\partial t}+\frac{\partial (F^i-F^v)}{\partial x}+\frac{\partial (G^i-G^v)}{\partial y}=0 \qquad (1)$$

Where $Q=(\rho,\rho u,\rho v,E)$ is the vector of conserved variables, F^i and G^i represent the convective fluxes and F^v and G^v describe the effect of viscous diffusion. Here ρ, u, v and E denote the density, Cartesian velocity components and total energy respectively.

Consider a control volume Ω with boundary $\partial\Omega$ which moves with Cartesian velocity components x_t and y_t. The equations of motion of the fluid can then be written in the integral form as:

$$\frac{d}{dt}\iint_\Omega Q\,dA+\oint_{\partial\Omega}((F^i-F^v)dy-(G^i-G^v)dx)=0 \qquad (2)$$

Where

$$F^i=\begin{pmatrix}\rho U\\ \rho uU+p\\ \rho vU\\ (\rho E+p)U+x_t p\end{pmatrix},G^i=\begin{pmatrix}\rho V\\ \rho uV\\ \rho vV+p\\ (\rho E+p)V+y_t p\end{pmatrix}$$
$$F^v=\begin{pmatrix}0\\ \tau_{xx}\\ \tau_{xy}\\ u\tau_{xx}+v\tau_{xy}+q_x\end{pmatrix},G^v=\begin{pmatrix}0\\ \tau_{xy}\\ \tau_{yy}\\ u\tau_{xy}+v\tau_{yy}+q_y\end{pmatrix} \qquad (3)$$

And the contravariant velocities are defined as:

$$U=u-x_t,\qquad V=v-y_t \qquad (4)$$

τ_{xx},τ_{xy} and τ_{yy} are the stress tensor and q_x and q_y are the heat flux vector components. The coefficient of viscosity, μ, is calculated according to Sutherland's law. Also, for an ideal gas, the equation of state may be written as

$$P = (\gamma - 1)\rho\left[E - \frac{1}{2}(u^2 + v^2) \right] \qquad (5)$$

Turbulence effects can be taken into account by use of a suitable turbulence model. In this work a two-equation $k-\varepsilon$ model is used. The turbulent transport equations can be written in a form similar to that used for the mean-flow equations

$$\frac{\partial Q_t}{\partial t} + \frac{\partial (F_t^i - F_t^v)}{\partial x} + \frac{\partial (G_t^i - G_t^v)}{\partial y} = S_t \qquad (6)$$

Where $Q_t = (\rho k, \rho\varepsilon)$, F_t^i and G_t^i represent the turbulent convective fluxes and F_t^v and G_t^v describe the effect of turbulent viscous diffusion. The source term S_t describes production and dissipation of turbulence quantities.

$$F_t^i = \begin{pmatrix} \rho U k \\ \rho U \varepsilon \end{pmatrix}, \quad G_t^i = \begin{pmatrix} \rho V k \\ \rho V \varepsilon \end{pmatrix}$$
$$F_t^v = \begin{pmatrix} \beta_{kx} \\ \beta_{\varepsilon y} \end{pmatrix}, \quad G_t^v = \begin{pmatrix} \beta_{ky} \\ \beta_{\varepsilon y} \end{pmatrix} \qquad (7)$$

Where

$$\beta_{kx} = -\left(\mu + \frac{\mu_t}{\sigma_k}\right)\frac{\partial k}{\partial x}, \quad \beta_{ky} = -\left(\mu + \frac{\mu_t}{\sigma_k}\right)\frac{\partial k}{\partial y}$$
$$\beta_{\varepsilon x} = -\left(\mu + \frac{\mu_t}{\sigma_\varepsilon}\right)\frac{\partial \varepsilon}{\partial x}, \quad \beta_{\varepsilon y} = -\left(\mu + \frac{\mu_t}{\sigma_\varepsilon}\right)\frac{\partial \varepsilon}{\partial y} \qquad (8)$$

Then the turbulent eddy viscosity is calculated from:

$$\mu_t = C_\mu \rho \frac{k^2}{\varepsilon} \qquad (9)$$

The following standard values, obtained empirically from experiments, are usually employed:

$C_\mu = 0.09, C_{\varepsilon 1} = 1.44, C_{\varepsilon 2} = 1.92, \sigma_k = 1, \sigma_\varepsilon = 1.3$

Note that in the present work the turbulence equations are solved with the main flow equations in a fully-coupled manner. This method provides better solution accuracy and convergence compared with the sequencing approach. Applying equation (1) independently to each cell in the mesh, the spatial and time dependent terms are decoupled and a set of ordinary differential equations is obtained in the following form:

$$\frac{d}{dt}(Q_i A_i) + E_i(Q) + NS_i(Q) - D_i(Q) = 0 \qquad (10)$$

Where, A_i is the cell area, $E_i(Q)$ are the convective fluxes and $NS_i(Q)$ are the viscous fluxes. The properties over each cell edges are evaluated using an averaging method. Following Jameson [9] in order to prevent oscillations in the neighborhood of shock waves and to provide background dissipation to suppress odd-even modes a blend of first and third-order dissipative $D_i(Q)$ is added. These dissipative terms provide an upwind bias and are added in the form of dissipative fluxes for conservation purposes with coefficients that depend on the local pressure gradient.

4 Implicit Time Integrations

The set of equation 10 can be integrated in time by using a fully implicit time discretisation (in real time) [2] to give:

$$\frac{d}{dt}(A_i^{n+1} Q_i^{n+1}) + R_i(Q^{n+1}) - D_i(Q^{n+1}) = 0 \qquad (11)$$

Where R is the sum of the two fluxes contributions. The superscript $n+1$ denotes the time level of the approximation and the d/dt operator is approximated by an implicit backward difference formula of kth-order accuracy of the form:

$$\frac{\mathrm{d}}{\mathrm{dt}} = \frac{1}{\Delta \mathrm{t}} \sum_{\mathrm{q}=1}^{\mathrm{k}} \frac{1}{\mathrm{q}} \left[\Delta^-\right]^{\mathrm{q}} \qquad (12)$$

Where

$$\Delta^- Q_i^{n+1} = Q_i^{n+1} - Q_i^n \qquad (13)$$

In the present work a second order time discretisation is used so equation 11 becomes:

$$\frac{3}{2\Delta \mathrm{t}}(\mathrm{A_i^{n+1}Q_i^{n+1}}) - \frac{2}{\Delta \mathrm{t}}(\mathrm{A_i^{n}Q_i^{n}}) + \frac{1}{2\Delta \mathrm{t}}(\mathrm{A_i^{n-1}Q_i^{n-1}}) + \mathrm{R_i(Q^{n+1})} - \mathrm{D_i(Q^{n+1})} = 0 \qquad (14)$$

Time accuracy can be further enhanced by using a third-order implicit time discretisation rather than the second-order discretisation used here. However, this is achieved at the expense of additional storage for an extra time level of accuracy, which is not always necessary considering the reasonable good accuracy obtained in general with second-order time discretisation. Equation (14) is nonlinear for Q^{n+1} and therefore cannot be solved analytically. At this stage, it is convenient to redefine a new residual R^*, referred to as unsteady residual, as following:

$$R^*(Q^{n+1}) = \frac{3}{2\Delta t}(A_i^{n+1}Q_i^{n+1}) - \frac{2}{\Delta t}(A_i^n Q_i^n) + \frac{1}{2\Delta t}(A_i^{n-1}Q_i^{n-1}) + R_i(Q^{n+1}) - D_i(Q^{n+1}) \quad (15)$$

The new equation can be seen as the solution of a steady state problem, which can then be solved with a time marching method by introducing derivative with respect to a fictitious pseudo-time τ:

$$A_i \frac{\partial Q_i^{n+1}}{\partial \tau} + R_i^*(Q^{n+1}) = 0 \quad (16)$$

The pseudo-time problem can then be solved by using any time-marching method designed to solve steady-state problems, utilizing standard acceleration techniques. In the present work an explicit four-stage Runge-Kutta method with local pseudo-time stepping and residual smoothing is used as follows:

$$\begin{aligned} Q^{(0)} &= (Q_i^{n+1})^m \\ Q^{(1)} &= Q^{(0)} - \frac{1}{4}\frac{\Delta\tau}{A_i}R_i^*(Q^{(0)}) \\ Q^{(2)} &= Q^{(0)} - \frac{1}{3}\frac{\Delta\tau}{A_i}R_i^*(Q^{(1)}) \\ Q^{(3)} &= Q^{(0)} - \frac{1}{2}\frac{\Delta\tau}{A_i}R_i^*(Q^{(2)}) \\ Q^{(4)} &= Q^{(0)} - \frac{\Delta\tau}{A_i}R_i^*(Q^{(3)}) \\ (Q_i^{n+1})^{m+1} &= Q^{(4)} \end{aligned} \quad (17)$$

Where the superscript m denotes the pseudo-time level $m\Delta\tau$ and

$$R^*(Q^L) = \frac{3}{2\Delta t}(A_i^{n+1}Q_i^L) - \frac{2}{\Delta t}(A_i^n Q_i^n) + \frac{1}{2\Delta t}(A_i^{n-1}Q_i^{n-1}) + R_i(Q^L) - D_i(Q^{n+1}) \quad (18)$$

It should be noted that for computational efficiency, the dissipative operator is frozen at the value of the first stage. The pseudo-time step is restricted by stability consideration. The allowable pseudo-time step for each cell is chosen using

$$\Delta\tau_i = \min\left[\frac{CFL\ A_i}{\sum_{j=1}^{3}\lambda_j}, \frac{2\Delta t}{3}\right] \quad (19)$$

Where

$$\lambda = u\Delta y - v\Delta x \quad (20)$$

In the present work the local pseudo-time stepping and residual smoothing are used to accelerate convergence. The real-time step can be chosen based on accuracy considerations.

5 Geometric Conservation Law

When computing the flow on a moving grid, the cell areas also vary in time and it is therefore important to discretise the time-dependent metrics carefully in order to maintain the conservative properties of the scheme. If the cell areas are calculated analytically in terms of the grid node positions, numerical errors will be introduced in the solution algorithm, which will increase with time. This is because the mesh motion is only approximately solved in the integration scheme. To avoid such numerical errors, the cell areas must be integrated forward in time by using the same method as that used to solve the physical conservation laws [10]. This is achieved by introducing a Geometric Conservation Law (GCL) which is derived from the continuity equation as follows:

$$\frac{\partial}{\partial t}\iint_{\Omega} dA - \oint_{\partial\Omega} v_g .n = 0 \qquad (21)$$

Where, A is the cell area, v_g is the grid speed and n is the normal area vector. Using the same second-order time discretisation as for the flow equation, Equation (21) becomes:

$$\frac{3A_i^{n+1} - 4A_i^n + A_i^{n-1}}{2\Delta t} - V_i^{n+1} = 0 \qquad (22)$$

Where

$$V_i^{n+1} = \sum_{j=1}^{3} x_{t_j}^{n+1}\Delta y_j^{n+1} - y_{t_j}^{n+1}\Delta x_j^{n+1} \qquad (23)$$

And hence

$$A_i^{n+1} = \frac{4A_i^n - A_i^{n-1} + 2\Delta t V_i^{n+1}}{3} \qquad (24)$$

The above geometric conservation laws must be satisfied at all time on the moving grid. This law states that the change in area of each control volume between t^n and t^{n+1} must be equal to the area swept by the cell boundary during $\Delta t = t^{n+1} - t^n$. Using the GCL to calculate the areas rather than calculating them geometrically ensures that large errors are not encountered when solving the physical conservation law. This formally introduces an error into the values obtained for the areas, but this is small in comparison with the numerical error in the solution procedure. The GCL needs to be evaluated only once every global time step to calculate the new cells area.

6 Boundary Conditions

At the airfoil surface, the no-slip boundary condition, need to be imposed. This is easily achieved by setting the velocity component to zero on the surface of the airfoil. Since the flow solver is based on a cell centered discretisation of the governing equations, the value of the pressure at the airfoil surface can be obtained by extrapolating from the values of adjacent cells. In the far-field, non-reflecting boundary conditions based on characteristic analysis are used. The wall function conditions are also considered for near wall turbulent calculations.

7 Results

A series of high Reynolds number unsteady transonic flows over the pitching airfoils are considered from the AGARD experimental test cases [11].

The first case is the CT5 case for NACA0012 airfoil. For this case, the periodic motion of the airfoil is defined by the angle of attack as a function of time as:

$$\alpha(t) = \alpha_m + \alpha_\circ \sin(\omega t) \qquad (25)$$

Where α_m is the mean incidence, $\alpha_\circ$ is the amplitude of the pitching oscillation and ω is the angular frequency of the motion which is related to the reduced frequency k by:

$$k = \frac{\omega c}{2U_\infty} \qquad (26)$$

Where c is the airfoil chord and U_∞ is the free-stream velocity. For all cases, the airfoil oscillates about its quarter chord.

The flow conditions over the airfoil are as follows:

$$M_\infty = 0.755,\ \alpha_m = 0.016,\ \alpha_0 = 2.51,\quad k = 0.0814,\qquad \mathrm{Re} = 5.5\times10^6 \qquad (27)$$

This case is a challenging test case due to a higher value of the Mach number which may make the viscous effects more significant. The flow is characterized by the presence of a strong shock wave, which develops alternatively on the upper and lower surface of the airfoil.

Comparison of the viscous and inviscid predicted pressure distributions with the experimental data is shown in figure 3 for four different incidences during the cycle. An over-prediction of the pressure jump across the shock wave is observed for inviscid solutions however, the viscous results show smeared more accurate shock predictions. Three unstructured grids are used for grid study calculations. The number of cells for coarse, medium and fine grids are 8829, 13487 and

15304 respectively. The comparison of the normal force and moment coefficients with the experimental data is shown in figure 4 for these three grids. As illustrated no significant difference can be seen between the medium and fine grids. Therefore, the medium grid is chosen for calculations in this paper. Another important issue in the dual-time method is proper selection of pseudo-time, steady-state error. Numerical experiments showed that this parameter effects on the accuracy of the solutions and the computational time. If the large values are used for this parameter, as shown in figure 5 the accuracy of the solution becomes very poor, and in contrast the small values, considerably increased the computational time. The case study in the present work has shown that the optimum value for pseudo-time, steady-state error has been in order of 10^{-3}. The effect of number of real time steps per period (Npp) on the accuracy of the solution is shown in figure 6. As illustrated, even reasonably low Npp, i.e. 30, can lead to accurate results.

The second case is the case CT6 of NACA64010 pitching airfoil. For this case, the periodic motion of the airfoil is defined as follow:

$$\alpha(t) = \alpha_m + \alpha_\circ \cos(\omega t) \qquad (28)$$

And the flow conditions are defined as:

$$M_\infty = 0.796,\ \alpha_m = 0.0,\ \alpha_0 = 1.01,\quad k = 0.202,\qquad \mathrm{Re} = 12.56\times 10^6 \qquad (29)$$

The generated grid for this airfoil is shown in figure 1 with 10392 cells in the domain and 217 nodes on the airfoil surface. Comparison of lift coefficient and pitching moment coefficient with experimental data and inviscid results is shown in figure 7. As shown the inclusion of viscous effects tilts the inviscid oval in the direction of the experimental results. Figure 8 shows the motion of the shocks in the upper and lower surfaces of the airfoil for a pitching cycle. As the airfoil pitches up, the shock in the upper surface moves aft at the same time as it becomes stronger. The shock in the lower surface moves forward, weakens, and disappears. As the airfoil pitches down, the opposite begins to happen, with a small phase lag.

7 Conclusions

The capability of an implicit time-accurate algorithm for the solution of two-dimensional compressible Navier-Stokes equations on unstructured moving grid has been demonstrated. The results obtained confirm the applicability of the current time stepping strategy, which combines an implicit dual-time approach to discretise the unsteady equations with an explicit time stepping method for solution of the steady state problem in pseudo-time. The method was incorporated within an unstructured mesh and was used in conjunction with a general moving grid technique, which allows rapid and efficient deformation of the grid in the case of different geometries. Results were presented for several pitching airfoil flows and good agreements were noted with experimental results. Considerable computational savings are also achieved using the present implicit scheme over fully explicit method.

References

[1] Batina J.T. Unsteady Euler algorithm with unstructured dynamic mesh for complex-aircraft aerodynamic analysis. *AIAA Journal*, Vol 29, No. 3, 1991.

[2] Jameson A. Time dependent calculations using multigrid with applications to unsteady flows past airfoils and wings. *AIAA Paper* 91-1596, 1991.

[3] Gaitonde A.L. A dual-time method for the solution of the unsteady Euler equations. *Aeronautical Journal*, October 1994, pp283-291.

[4] Alonso J, Martinelli L and Jameson A. Multigrid unsteady Navier-Stokes calculation with aeroelastic aplication. *AIAA paper*, 95-004.

[5] Badcock K.J, Cantariti F, Hawkins I, Gribben, B, Dubuc L, Richards B.E. Simulation of unsteady turbulent flows using the pseudo time method. *Aerospace Eng. Dept.* Rep. 9721, Glasgow Univ., 1997.

[6] Chassaing J.C, Gerolymos G.A. and Vallet I. Reynolds-Stress model dual-time-stepping

computation of unsteady 3-D flows. AIAA Journal, Vol 41, No. 10, pp 1882-1894, 2003.

[7] Jahangirian A. and Johnston L.J. Automatic generation of adaptive unstructured grids for viscous flow applications. 5th Int. Conf. *on Numerical Grid Generation in CFD*, Mississippi state university, 1996.

[8] Mavriplis D. and Mortinelli L. Multi grid solution of compressible turbulent flow on unstructured meshes using two-equation model. *Int. J. for Num. Meth. in Fluied*, Vol. 18,pp887-914, 1994.

[9] Jameson A. and Mavriplis D. Finite volume solution of the two-dimensional Euler equation on a regular triangular mesh. *AIAA Journal*, Vol.24, NO.4, April 1986.

[10] Ilinca A. and Ilinca C. Geometric conservation laws for three-dimensional unstructured moving grid. *CFD 98*.

[11] Compendium of Unsteady Aerodynamic Measurements. AGARD, R-702, 1982.

[12] Gaitonde A.L, Fiddes S.P. A comparison of a cell-center method and a cell-vertex method for the solution of the two-dimensional unsteady Euler equations on a moving grid. *Journal of aerospace Engineering*, Vol. 209, 1995, 203-213.

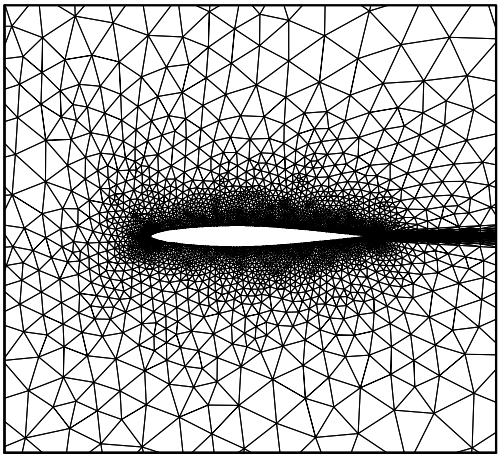

Fig. 1. Computational grids over NACA64010 airfoil

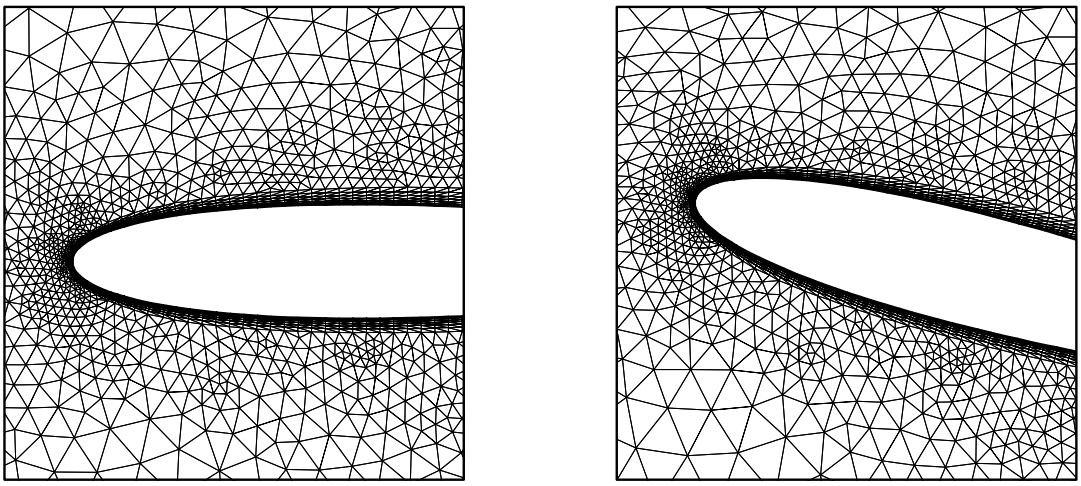

Fig. 2. Grid movement strategy for viscous grids (left before and right after movement)

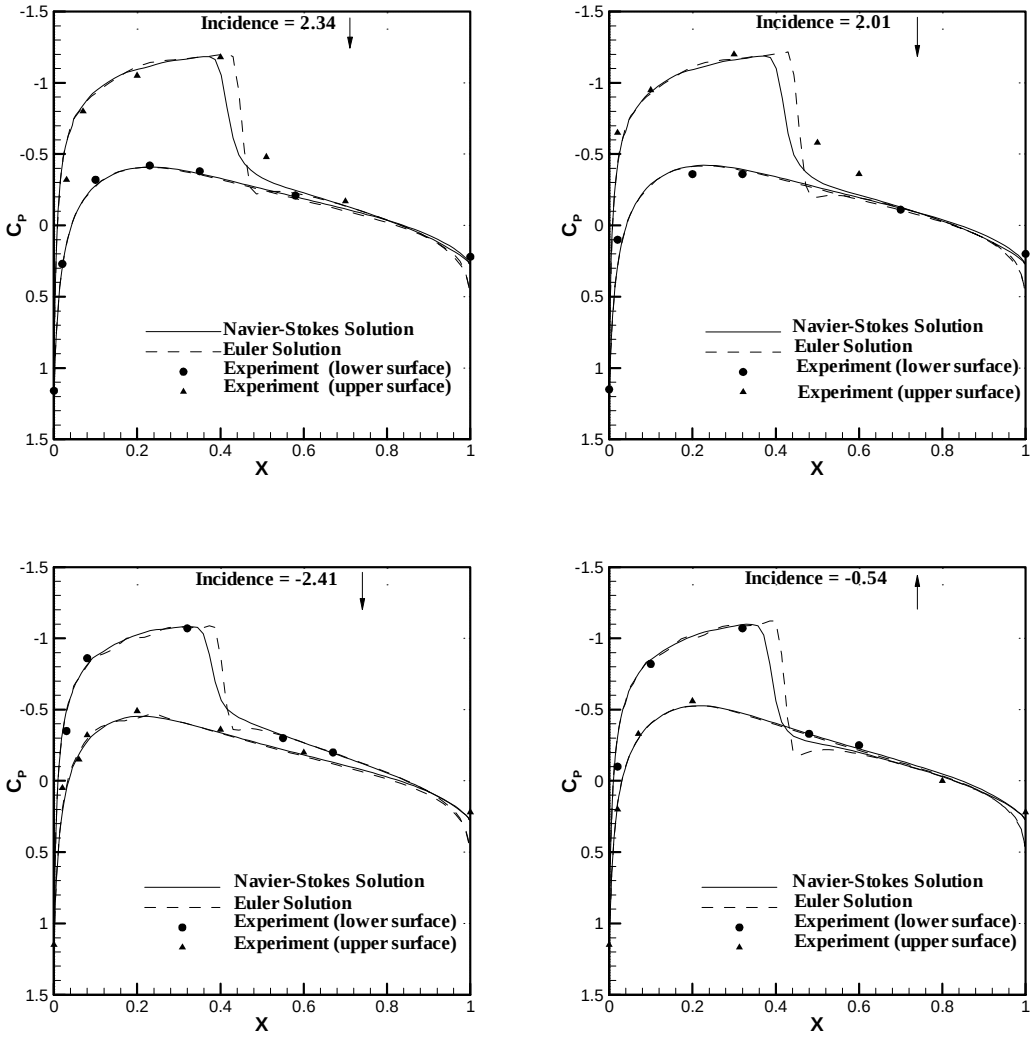

Fig. 3. Instantaneous pressure distribution for NACA0012, test case CT5

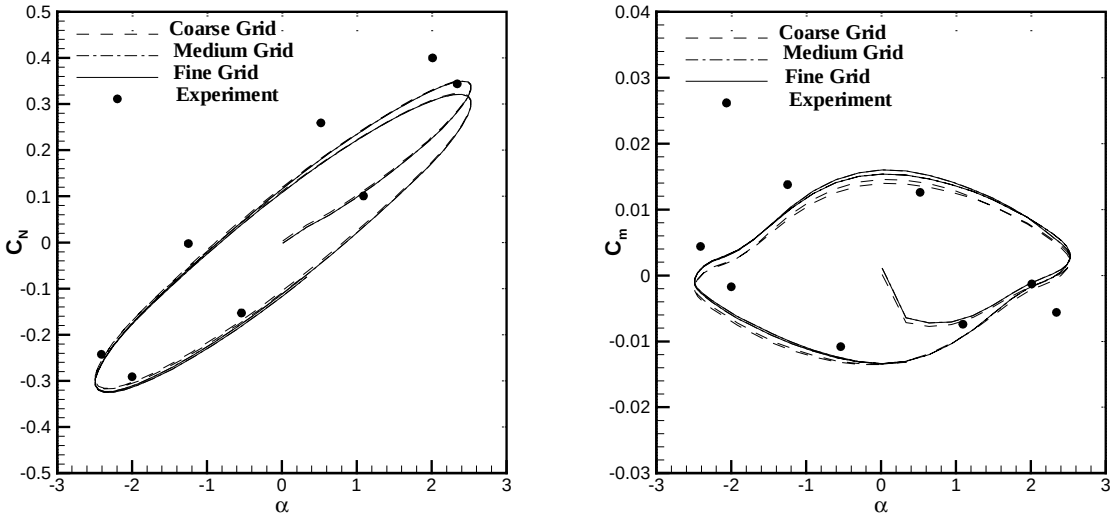

Fig. 4. Normal force and pitching moment coefficient loops for NACA0012, test case CT5

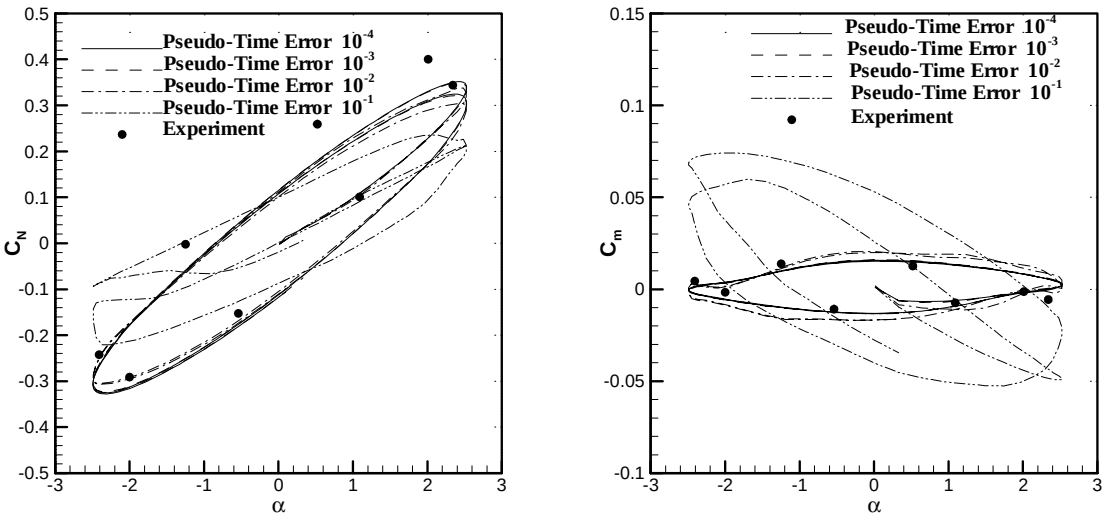

Fig. 5. Effect of pseudo-time error on the accuracy of solution

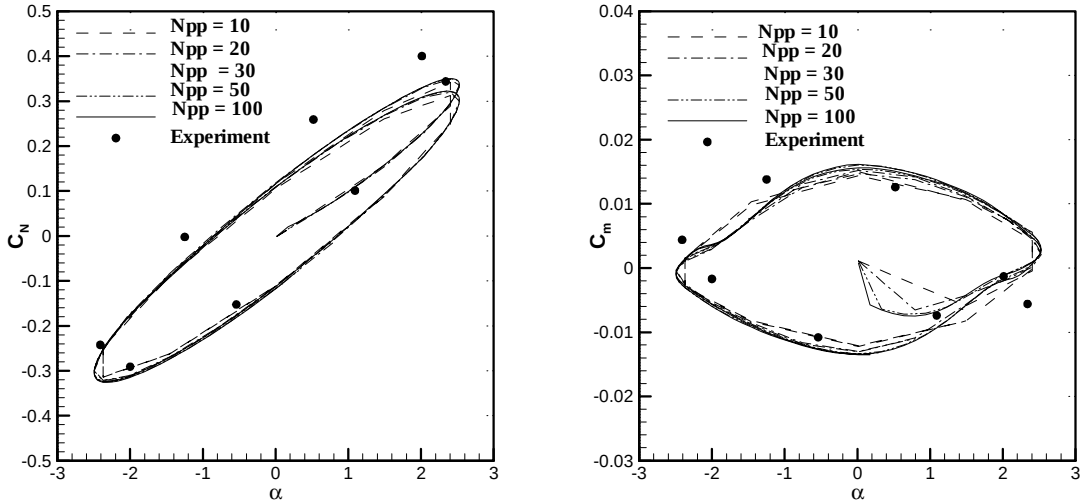

Fig. 6. Effect of number of steps per cycle (Npp) on the accuracy of solution

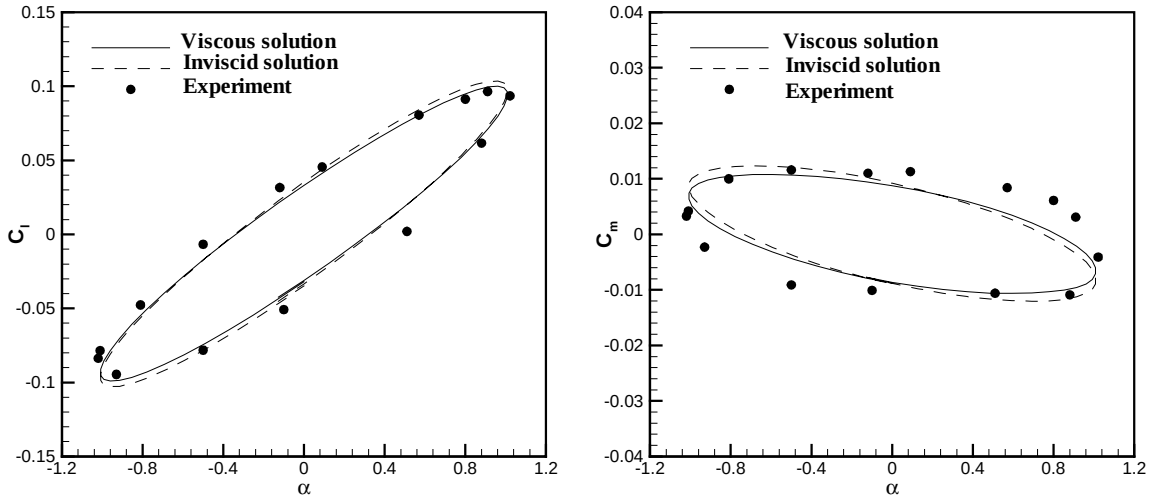

Fig. 7. Normal force and pitching moment coefficient loops for NACA64010, test case CT6

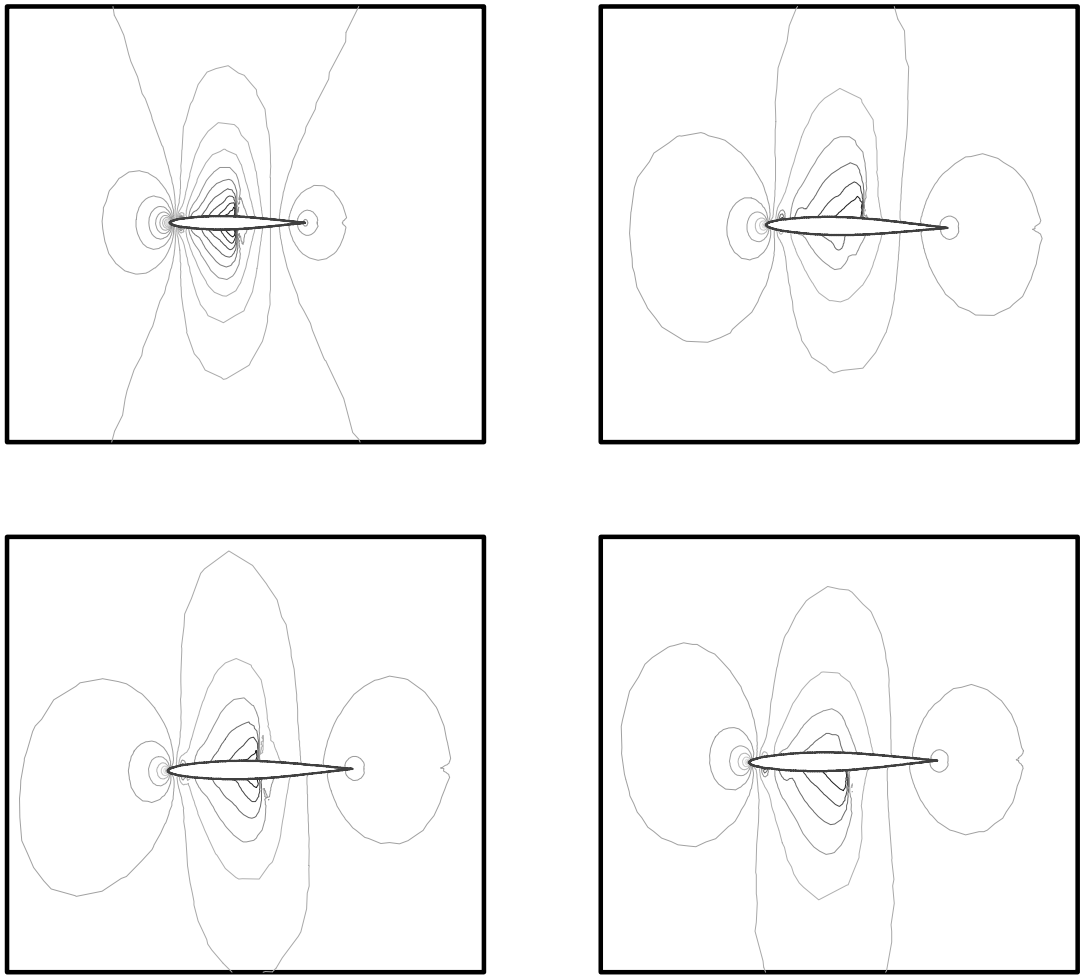

Fig. 8. . Instantaneous pressure contours for NACA64010, test case CT6